A generalized heat-transfer model for shielded-fire household cookstoves

CrossMark

Nordica A. MacCarty [a,*], Kenneth M. Bryden [b]

[a] Oregon State University, School of Mechanical, Industrial and Manufacturing Engineering, 204 Rogers Hall, Corvallis, OR 97331, USA
[b] Iowa State University, Department of Mechanical Engineering, 1620 Howe Hall, Ames, IA 50011-2274, USA

ABSTRACT

This paper presents an experimentally validated steady-state heat transfer model of a shielded-fire, natural-draft biomass cookstove suitable for conceptual design of the small household cookstoves used in developing countries. The input variables for the model included 10 geometrical design variables, 2 material design variables, and 3 operating conditions. This model was validated using data from three previously published studies including 63 distinct combinations of the 15 design variables. The model results for thermal efficiency are within $\pm 5\%$ for 59 of the 63 designs and have an L2 norm error of 3.0%. Parametric variations of design variables can assist in the conceptual phase of design. In addition, the temperature and velocity profiles, location and magnitude of losses, and heat transfer contributions through various modes and regions of the pot provide sufficient detail to improve the understanding of a cookstove system and support detailed design.

© 2016 International Energy Initiative. Published by Elsevier Inc. All rights reserved.

Introduction and background

Approximately 2.7 billion people use solid biomass fuel in small stoves and three-stone fires to meet their household energy needs for cooking each day (IEA, 2010). This results in a number of adverse health, safety, community, and environmental effects including 4 million premature deaths each year, deforestation, and climate-changing emissions (Lim et al., 2012; Rehfuess, 2006; IEA, 2010; Bond and Sun, 2005). Recent projections indicate that use of biomass for cooking will increase and continue to be the dominant energy use in rural households through 2030 (IEA, 2010; Daioglou et al., 2012). For example recent studies in the West African Sahel found that in rural villages 98% of household energy needs are met with small household cookstoves (Johnson and Bryden, 2012a, 2012b). For these subsistence-level families, the cost of acquiring biomass fuel to meet their household energy needs represents a significant fraction of time and income (Rehfuess, 2006). As a result the design, manufacture, and distribution of clean, low cost, high efficiency household cookstoves has been identified by many governmental and non-governmental organizations as a critical need to improve the lives of the resource-poor while concurrently addressing millennium development goals and slowing climate change.

To meet this need a number groups have over the past thirty years worked to research, develop, and design household cookstoves, with more than 160 stove projects currently operating worldwide (Ruiz-Mercado et al., 2011). In spite of this the design of cookstoves today is primarily a heuristic trial and error process based on previous experience, engineering judgment, rules of thumb, and experiment. Currently there is no dominant design basis or established design algorithm for optimizing the efficiency of these devices, nor are there validated and accepted models or modeling guidelines to support the design process. In addition, there is no standard methodology for stove testing and reporting such that experimental data can be used for model development and validation. Over the past 30 years fewer than 30 journal articles have been written on the computational modeling of household biomass cookstoves, with the majority of these activities focusing on a single stove design, and few of these provide detailed experimental validation of the computational results (MacCarty and Bryden, 2015a). This paper presents an experimentally validated model capable of predicting the heat transfer performance of small cookstoves over a wide range of combustion conditions and geometric variables.

As shown in Fig. 1, a typical natural draft biomass cooking stove is conceptualized as being composed of the air handling system, the combustion chamber, the convective heat transfer region, the cooking pot, and the support structure and insulation. For modeling purposes, this system can be divided into three zones: the solid phase packed bed zone, the gas phase combustion or flame zone, and the heat transfer zone. In the packed bed, solid phase combustion includes heating and drying of the wood followed by pyrolysis and char combustion with primary air. In the flame zone, secondary air enters, is heated, and is supplied to the gas phase combustion. In the heat transfer zone, energy is lost through the stove walls, transferred to the pot via convection and

* Corresponding author.
E-mail address: Nordica.MacCarty@oregonstate.edu (N.A. MacCarty).

Nomenclature

A	Area
c_p	Specific heat
D	Diameter
D_h	Hydraulic diameter
F	View factor
f	Friction factor
g	Gravity
H	Height
h	Specific enthalpy
$\tilde{h}$	Convective heat transfer coefficient
h_{fg}	Latent heat of vaporization
i	Counter, species flow in bed zone
j	Counter, incoming species in flame zone
k	Counter, total species flow of gases
$\tilde{k}$	Thermal conductivity
l	Counter, pressure losses
K	Pressure loss coefficient
$\dot{m}$	Mass flow
q	Heat transfer rate
R	Thermal resistance
T	Temperature
V	Velocity
W	Width
x	Segment length
β	Fuel bed size factor
ε	Emissivity
η	Thermal efficiency
ρ	Density
σ	Stefan-Boltzmann constant
ϕ	Radiation heat transfer adjustment factor
Nu	Nusselt number
Pr	Prandtl number
Re	Reynolds number
HHV	Higher heating value

Subscripts

air2	secondary air
amb	ambient
bed	fuel bed
c	combustion chamber
char	char
cond	conduction
cont	contraction
exp	expansion
ext	exterior wall
flame	flame
in	inlet
int	interior wall
pot	pot
rad	radiation
s	stove
sh	shield
v	volatiles
w	water
wall	wall

Initial modeling efforts in the 1980s included algebraic and differential zonal models of open fires, shielded-fire stoves, and enclosed stoves, and focused on identifying equation sets for fluid flow and heat transfer throughout the system (De Lepeleire et al., 1981; Bussmann and Prasad, 1982; Bussmann et al., 1983; Bussmann and Prasad, 1986; Prasad et al., 1985). This was followed by investigation of specific regions such as wall losses or heat transfer correlations within a pot shield (Baldwin, 1987), or models of a specific stove design (Date, 1988; Kumar et al., 1990). After 2010, researchers continued to algebraically model specific stove designs (Agenbroad et al., 2011a, 2011b; Zube, 2010) and some incorporated solid and gas phase combustion rates and efficiency (Shah and Date, 2011). Several researchers have used CFD packages for stove modeling (Burnham-Slipper, 2007a, 2007b, 2008; Gupta and Mittal, 2010a, 2010b; Joshi et al., 2012; Ravi et al., 2002; Ravi et al., 2004) or for investigating heat transfer in specific regions of the stove (Wohlgemuth, 2010; Urban et al., 2002; McCorkle et al., 2003; Bryden et al., 2003). Hannai et al. (2006) used a neural network based model to predict the thermal efficiency of cooking pots based on experimental data for varying pot radii, height, degree of curvature, material conductivity, and flame diameter. This model was then validated using separate experiments and used to determine the effects of different parameters on efficiency. As a result, the optimal cooking pot could be designed for a given situation, similar to the present goal with cookstoves. A more detailed discussion of past biomass cookstove modeling efforts is presented in the recent review by MacCarty and Bryden (2015a).

Model development

As noted earlier, due to the lack of a suitable and accessible equation set, the current stove design process does not involve the assistance of computational modeling during the conceptual design phase, resulting in a missed opportunity for greater speed and accuracy in arriving at the most efficient design. To fill this gap, this paper presents a validated model for prediction of the steady-state thermal efficiency of a cylindrical, shielded-fire household cookstove with a natural draft air supply and flat-bottomed metal pot of diameter larger than the combustion chamber burning a continuous feed of wood sticks as fuel. Following a review of the literature, this general design was chosen as representative of the most common existing improved stove designs available today as shown by stove testing catalogs (Jetter et al., 2012; MacCarty et al., 2010) and in-field studies. While cookstoves using prepared fuels or forced draft may offer good performance, these will require modifications to modeling techniques and data for validation and are therefore left for a later time. The present model is based on a review of past modeling efforts of heat transfer and fluid flow, and validated using 63 data points of experimental results from three previously published studies catalogued in (MacCarty and Bryden, 2015b).

The model utilizes 15 operational, geometrical, and material design variables as inputs. The operating conditions include a constant given firepower, fuel heating value and as-received moisture content. The stove material and geometry are described by 12 design variables (Fig. 2):

- D_c—combustion chamber diameter
- H_c—combustion chamber height
- W_c—gap at the edge of the combustion chamber
- W_p—gap at the edge of the pot bottom
- W_{sh}—gap between shield (if included) and pot
- D_p—pot diameter
- H_p—height of water in the pot based on water volume
- D_s—stove combustion chamber body diameter
- k_s—stove body material conductivity (can account for multiple material layers via thermal resistance)
- H_{sh}—height of shield, if included

radiation, and exits as sensible losses. Fluid flow and the entrainment of excess air are driven by natural buoyancy, and is slowed by pressure losses due to friction throughout the various geometries of the flow path.

Three types of cookstove models have been developed by researchers: integral or zonal models, CFD models, and neural networks.
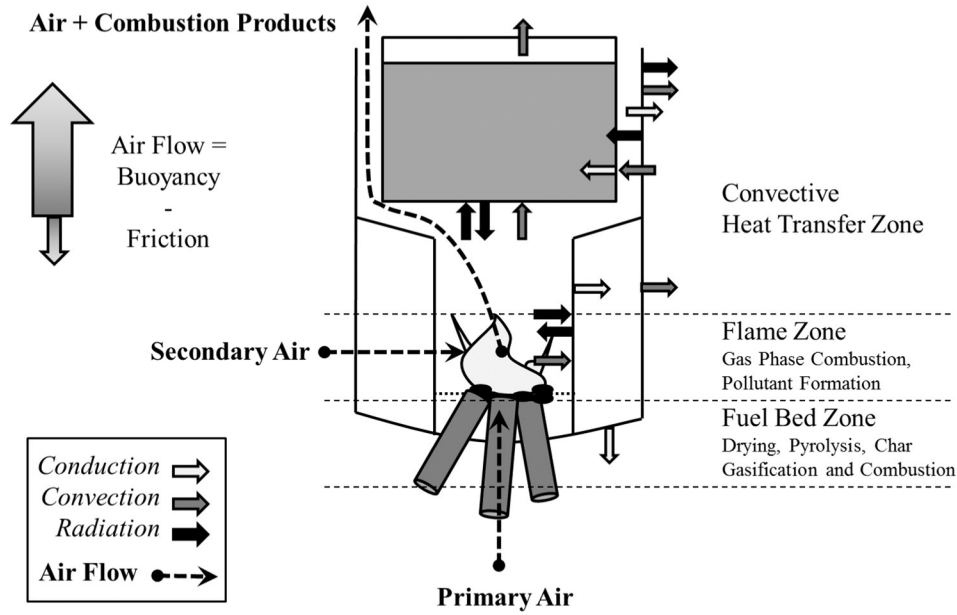
Fig. 1. Combustion, flow, and heat transfer processes (adapted from MacCarty and Bryden, 2015a)

- t_{sh}—thickness of shield material
- k_{sh}—shield material conductivity

Based on the experimental results available and current design and testing, the following assumptions are made:

- The operation is steady state.
- The firepower is given and sets the combustion rate.
- The fuel bed receives moist wood and underfire air as inputs. The wood is dried and pyrolyzed in the fuel bed producing water vapor, pyrolysis gases, and char. The char is combusted with oxygen to form carbon dioxide. The underfire air is stoichiometric with respect to the char combustion.
- The gases leaving the fuel bed leave at the temperature of the top surface of fuel bed.

Fig. 2. Stove geometry.

- The fuel bed covers the entire bottom of the combustion chamber, which is assumed to be adiabatic.
- The pyrolysis gases are completely combusted with the overfire air.
- The thermodynamic properties of the combustion gases except for water vapor from fuel moisture are the same as air.
- Airflow within the combustion chamber is axisymmetric, one-dimensional, and vertical.
- The radial temperature is uniform in the theta direction.
- Radiation heat transfer is idealized with radiant heat transfer only between surfaces with non-participating media. A radiation heat transfer adjustment factor, ϕ, of 0.2 is introduced to account for view blockage and non-ideal radiative heat transfer.
- In the cases where the combustion chamber and stove top include multiple layers (such as metal surrounding insulation), conduction is determined through as total thermal resistance or taken as the material with the lowest thermal conductivity.
- The pot is a flat-bottomed, metal pot.
- Combustion constants and properties are shown in Table 1.
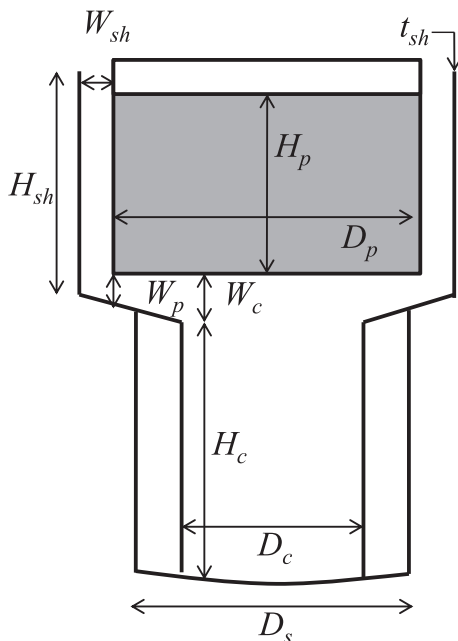
The model determines heat transfer and losses via the energy balance in the elements within each of the three zones within the stove.

Within the packed bed, the feed rate of wood fuel is set by the assumed firepower. The underfire air is stoichiometric with respect to the char produced. The wood fuel is dried, pyrolyzed, and char combusted at a rate consistent with the feed rate of wood. The mass flow rate and enthalpy of wood, water vapor from fuel moisture, and gases (including air, pyrolysis, and carbon dioxide from char combustion) are tracked separately. The hot gases from the fuel bed enter the flame zone where they are mixed with the overfire air. The gas species except for the water vapor are assumed to have the same thermodynamic properties of air. An energy balance (Eq. (4)) in the bed zone is used to solve for the temperature of the gases leaving the bed (Bussmann et al., 1983; Bussmann and Prasad, 1986).

$$\dot{m}_{char}HHV_{char} = \sum_i \dot{m}_i\left(h_{bed,i} - h_{amb,i}\right) + \dot{m}_w h_{fg}$$
$$+ \phi_{flame}\varepsilon_{char}\sigma A_{bed}F_{bed-pot}\left(T_{bed}^4 - T_{pot}^4\right)$$
$$+ \phi_g\varepsilon_{char}\sigma A_{bed}\left(1 - F_{bed-pot}\right)\left(T_{bed}^4 - T_{wall}^4\right) \quad (4)$$

Table 1
Properties and constants.

Property	Value	Reference
Wood combustion	$CH_{1.48}O_{0.65} + 1.05(O_2 + 3.76N_2) \rightarrow CO_2 + 0.74H_2O + 3.93N_2$	Ragland and Baker (1991))
	$f_{(s)} = 0.166$	
	$AFR_{(s)} = 6.04$ (assumed for all experimental comparisons)	
	$LHV = HHV - (\frac{m_{H_2O}}{m_f})h_{fg}$ (1)	
	Where m_{H20} is the sum of water as moisture in the fuel and the water produced by the fuel hydrogen during combustion	
	$HHV_{f,dry} = 20$ MJ/kg (assumed unless specifically provided in (MacCarty and Bryden, 2015b)	
	$LHV_{dry} = y_{ch}HHV_{ch} + y_v LHV_v$ (2)	
Char combustion	$y_{ch} = 0.2$	Bussman et al. (1983); Bussmann and Prasad (1986);Prasad et al.
	$HHV_{ch} = 32.8$ MJ/kg (assuming all carbon)	(1985); Ragland and Baker (1991)
	$\lambda_{ch} = 1$	
	$C + (O_2 + 3.76N_2) \rightarrow CO_2 + 3.76N_2$ (3)	
Pot details	$T_p = 373$ K	
	$\varepsilon_p = 1.0$	
	$F_{b-p} =$ calculated per view factor of two parallel discs	
	$F_{stovetop-p} = 1.0$	
	$F_{sh-p} = 1.0$	
Gas properties	Conductivity: $k = -2 \cdot 10^{-8}T^2 + 8 \cdot 10^{-5}T + 0.0033$ W/m·K	EES (2011)
	Density: $\rho = \frac{353.09}{T}$ kg/m^3	
	Enthalpy: $h = 0.0725T^2 + 984.49T - 7265.9$ J/kg	
	Specific Heat: $c_p = 0.145T + 984.49$ J/kg·K	
	Viscosity: $\mu = -7 \cdot 10^{-12}T^2 + 4 \cdot 10^{-8}T + 8 \cdot 10^{-6}$ kg/m·s	
Constants	Specific heat of water vapor:	
	$c_{p,w} = -7E - 11T^3 + 2E - 7T^2 + 0.0005T + 1.6786$ kJ/kg·K	
	$g = 9.81$ m/s^2	
	$T_{amb} = 298$ K	
	$\sigma = 5.67E - 8$ W/m2 K^4	
	$h_{fg} = 2260$ kJ/kg	

In the flame zone, an energy balance (Eq. (5)) is used to determine the gas temperature at the inlet of the combustion chamber. It assumes instantaneous and complete combustion of the volatiles and no radiation loss from the flame.

$$\dot{m}_v HHV_v + \left[\sum_j [\dot{m}_j h_j]_{bed} + [\dot{m}_{air2}h_{air2}]_{amb} \right]_{in} = \sum_j [\dot{m}_j h_j]_{out} \qquad (5)$$
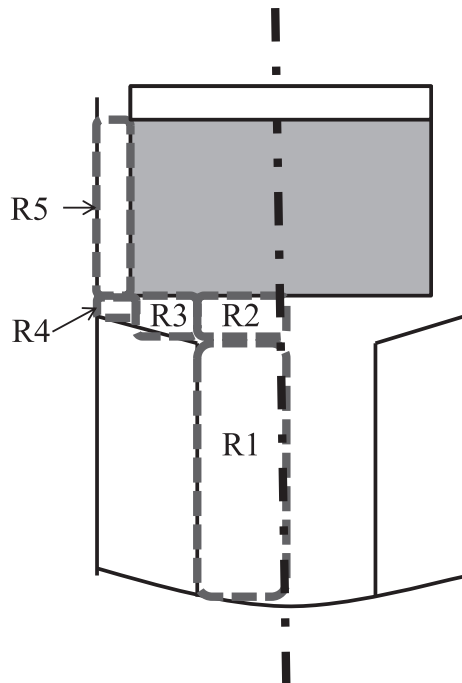
Hot gases from the flame zone enter the heat transfer zone, which is divided into five regions (Fig. 3). The combustion gases flow up through the combustion chamber (1), to the cooking pot center directly above the fuel bed and flame zone (2), to the cooking pot bottom beyond the edges of the combustion chamber (3), to the pot corner (4) and sides (5). Energy losses through the stove body and heat transfer to the pot are found by discretizing the energy conservation equation for each region. Regions 1, 3, and 5 are discretized into cylindrical or annular control volumes with user-defined thickness, Δx, while regions 2 and 4 are each a single volume. Radiation heat transfer is modeled assuming blackbody radiation between surfaces with non-participating media and a radiation heat transfer adjustment factor fitted from experimental data. Convective heat transfer coefficients in various regions are taken from the existing heat transfer relationships or fitted to published experimental results.

Fig. 3. Regions of the stove.

Region 1: combustion chamber

The combustion chamber is represented by control volumes as a series of stacked discs with vertical flow surrounded by the combustion chamber wall. Conservation of energy is used to determine the exit temperature of each volume (Eq. (6)), with the initial inlet temperature equal to the flame temperature. The energy balance includes radiation from the fuelbed to the wall, and radiation from the wall to the pot,

with the wall-to-wall radiation assumed net zero.

$$\sum_k \dot{m}_k(h_{flame,k} - h_{out,k}) = \phi_g \sigma A_{pot,rad} F_{pot\text{-}wall}\left(T_{int}^4 - T_{pot}^4\right)$$
$$+ \phi_{flame} \varepsilon_{char} \sigma A_{bed} F_{bed\text{-}wall}\left(T_{int}^4 - T_{bed}^4\right)$$
$$+ q_{wall} \tag{6}$$

Heat loss through the wall is represented by the analog model of thermal resistance (Eq. (7)). Here radiative transport is treated as an equivalent convective term. In the cases of stoves with metal combustion chamber and exterior walls filled with insulation, only the insulative layer is considered. Multiple layers of material can be considered using the sum of the conductive resistances of each layer.

$$q_{wall} = \frac{T_{in} - T_{amb}}{R_{int} + R_{cond} + R_{ext}} = \frac{T_{in} - T_{int}}{R_{int}} = \frac{T_{ext} - T_{amb}}{R_{ext}} \tag{7}$$

where

$$R_{int} = \frac{1}{\pi D_c H_c\left(\tilde{h}_{int} + \sigma \varepsilon_{char} A_{bed} F_{bed\text{-}wall}\left[\dfrac{\beta T_{bed}^4 + T_{pot}^4 - 2T_{int}^4}{T_{in} - T_{int}}\right]\right)} \tag{8}$$

$$R_{ext} = \frac{1}{\pi D_s H_c\left(1.42\left(\frac{T_{ext} - T_{amb}}{H_s}\right)^{0.25} + \sigma \varepsilon_{wall}\left[\dfrac{T_{ext}^4 - T_{amb}^4}{T_{ext} - T_{amb}}\right]\right)} \tag{9}$$

$$R_{cond} = \frac{\ln\left(D_s/D_c\right)}{2\pi H_c \tilde{k}_s} \tag{10}$$

Here a constant interior convective heat transfer coefficient of 10 W/m² K is used for the interior convective heat transfer coefficient (Baldwin, 1987). Alternatively this can be calculated using the empirical correlation for free laminar convection along a vertical heated plate in air, $\tilde{h} = 1.42(\Delta T/L)^{1/4}$ (Nag, 2006), as in the denominator of Eq. (9). Using the vertical heated plate correlation, the value for the interior convective heat transfer coefficient varies between 5.8–13.4 W/m² K with average 8.6 W/m² K and L2 error of 2.1 W/m² K from 10 W/m² K, representing an average change in predicted efficiency of 0.03% with maximum 0.3%. Therefore the constant value is used. Heat flow is initially calculated using the interior and exterior wall temperatures from the previous iteration, which are then updated and bisection is used to determine the exit temperature of the gas.

Region 2: pot bottom center

The single cylindrical region directly above the combustion chamber exit is treated as a stagnation point of average heat transfer to the pot only with no losses (Eq. (11)).

$$\sum_k \dot{m}_k(h_{in,k} - h_{out,k}) = \tilde{h}\pi\left(\frac{D_c}{2}\right)^2(T_{in} - T_{pot}) \tag{11}$$

The potential convective heat transfer correlations are presented in Table 2, including correlations from the literature (Eqs. (12)–(14)) or optimization of the form of Eq. (15). These correlations were investigated to determine which correlation gave best prediction of the experimental data set. Analysis concluded that the correlation from (Bussmann et al., 1983) (Eq. (14)) with $D_{plume} = D_c$ gave the best agreement of published options.

Region 3: pot bottom above stove body

This region consists of a series of coaxial annular rings of width Δx with a potentially sloped bottom which transfer heat to both the pot bottom through convection and radiation and stove body through convection and conduction (Eq. (16)).

$$\sum_k \dot{m}_k(h_{in,k} - h_{out,k}) = \tilde{h}A_{pot}(T_{in} - T_{pot}) + q_{wall} + \phi_g \sigma A_{pot}\left(T_{int}^4 - T_{pot}^4\right) \tag{16}$$

The view factor from the stovetop to pot bottom is assumed 1 (for infinite parallel plates), thus the area of the flat pot bottom is used for radiation calculations instead of the slightly sloped area of the stovetop and radiative heat transfer is neglected from the wall loss.

The convective heat transfer at the pot bottom is determined from the same two equation options as the center region (Eqs. (12) and (13)) or a correlation from Bussmann's open fire work (Bussmann et al., 1983) beyond the stagnation region (Eq. (17)).

$$Nu_{D_{plume}} = 0.32\,Pr^{0.33}Re_{D_{plume}}^{0.7}\left(\frac{r}{D_{plume}}\right)^{-1.23} \tag{17}$$

Or it is optimized with the form with either the same or different values of c_1, n_1, and n_2 relative to region 2 (Eq. (18)).

$$Nu = c_2 Re_{D_c}^{n_{12}}\left(\frac{D_p}{D_c}\right)^{n_{22}} \tag{18}$$

The convective heat transfer coefficient to the stovetop is assumed equal to that of the pot. Heat loss to the stovetop uses the same thermal resistance methods as region 1, with no radiation analog at the interior and conduction through the stove body ends at the cylindrical temperature profile determined at the exit of the combustion chamber (Eq. (19)) where $r = r_c + i\Delta x$. If the stovetop is sloped, the wall thickness begins at zero and increases to the outside of the stove (Eq. (20)). In the case of a stove with a body diameter smaller than that of the pot, thermal resistance through the stove wall thickness to ambient is used instead, including convection and radiation terms on each end.

$$T_{body,i} = T_{ext,H_c} - (T_{ext,H_c} - T_{int,H_c})\frac{\ln\left(r_s/r\right)}{\ln\left(r_s/r_c\right)} \tag{19}$$

$$t_{wall,i} = i\Delta x\frac{W_c - W_p}{r_p - r_c} \tag{20}$$

Region 4: pot corner

In the single region at the pot corner, there is no heat transfer into the pot but there are losses to the stove body and shield (Eq. (21)). Heat flux through the body is assumed to be equal to the wall flux in

Table 2
Options for Nu at the pot bottom center.

Method	Equation	
Entire pot bottom (Bussmann and Prasad, 1986)	$Nu_{D_{plume}} = 1.26\,,Pr^{0.42}Re_{D_{plume}}\left(\frac{D_p}{D_{plume}}\right)^{-0.5}$	(12)
Entire pot bottom (Shah and Date, 2011)	$Nu = 0.5(1.65Re_{D_c}^{0.5} + 2.733Re_{D_c}^{0.59})$	(13)
Stagnation region in open fire (Bussmann et al., 1983)	$Nu_{D_{plume}} = 1.03\,,Pr^{0.42}Re_{D_{plume}}^{0.5}\left(\frac{D_c}{D_{plume}}\right)^{-0.65}$	(14)
Optimization form	$Nu = c_1 Re_{D_c}^{n_{11}}\left(\frac{D_p}{D_c}\right)^{n_{21}}$	(15)

the final element of region 3. Heat flux through the shield in this region, if present, is assumed equal to the flux through the first element in region 5 from the previous iteration.

$$\sum_k \dot{m}_k (h_{in,k} - h_{out,k}) = q_{wall,stovetop} + q_{wall,shield} \tag{21}$$

Region 5: pot sides

At the pot sides the control volumes are a series of stacked annular rings of height Δx. The calculation of heat transfer ends at the height of the water. If the shield is higher than this level, this additional height is considered in the buoyancy calculations only. The sides of the pot have three possible conditions: 1) completely unshielded 2) within a shield and 3) in an unshielded region past the height of an existing shield. Possible convective heat transfer correlations are shown in Table 3, and the energy balance is shown by Eq. (22).

$$\sum_k \dot{m}_k (h_{in,k} - h_{out,k}) = \tilde{h}A_{pot}(T_{in} - T_{pot}) + q_{wall} + \phi_g \sigma A_{pot}\left(T_{int}^4 - T_{pot}^4\right) \tag{22}$$

Radiation from shield to pot is considered for the shielded regions with a view factor of 1 using the average interior shield temperature from the previous iteration. Heat flux through the shield wall is calculated using thermal resistance, assuming an equal interior convective heat transfer coefficient as that of to the pot and calculated per the heated plate equation on the exterior. The interior and exterior include a separate radiation term (Eqs. (31) and (32)) such that they are combined with the convective resistance at the interior or exterior (Eq. (33)) in parallel (Eq. (34)) (Baldwin, 1987), which is then combined in series with conduction through the shield in a method similar to that of the combustion chamber walls (Eq. (7)).

$$R_{rad,int} = \frac{1}{A_{sh,int}\tilde{h}_{rad,int}} = \frac{1}{A_{sh,int}\sigma\varepsilon(T_{sh,int} + T_p)\left(T_{sh,int}^2 + T_p^2\right)} \tag{31}$$

$$R_{rad,ext} = \frac{1}{A_{sh,ext}\tilde{h}_{rad,ext}} = \frac{1}{A_{sh,ext}\sigma\varepsilon(T_{sh,ext} + T_{amb})\left(T_{sh,ext}^2 + T_{amb}^2\right)} \tag{32}$$

$$R_{conv} = \frac{1}{\tilde{h}A_{sh}} \tag{33}$$

$$R_{rad+conv} = \frac{R_{rad}R_{conv}}{R_{rad} + R_{conv}} \tag{34}$$

Fluid flow

Fluid flow through the combustion chamber is determined by a momentum balance of airflow due to buoyancy and pressure losses through friction, bends, expansions, and contractions in the flow path (Eq. (35)) which is used to determine exit velocity and thus total mass flow of gas.

$$\frac{\rho_{exit}V_{exit}^2}{2} = g(H_c + W_c + H_{sh})(\rho_{amb} - \rho_{exit}) - \sum_l \rho_l \frac{V_l^2}{2}\left(\frac{f_l x_l}{D_{h,l}} + K_l\right) \tag{35}$$

The exit of the stove for buoyancy calculations is considered to be the point where the flow exits the shield surrounding the pot, or from under the pot in an unshielded stove. The flow path is treated similar to pipe flow and includes pressure drop through 1) the fuel bed, 2) 90° turn under the pot center, 3) gradual contraction or expansion from the combustion chamber along under the pot (the end of region 1 to end of region 3), 4) 90° turn at the pot corner, 5) contraction or expansion to the pot side, and 6) the friction throughout the channels per volume height. Equations for these are shown in Table 4. A number of possible correlations for K_{cont} along the bottom and side of the pot were available and are shown in Fig. 4. The variable pressure drop coefficient in the bed, K_{bed} was assumed zero for all stoves, as stoves of this type have generally been designed to have little air entry resistance with possibly limited flow through the grate but free flow of air above and around the fuel. An additional term of $K_{bed} = 0.75$ was incorporated into the Envirofit stove from (Jetter et al., 2012) to reflect the effect of the reducer ring within the combustion chamber. (See Fig. 5.)

The mass flow rate of gases is calculated initially assuming stoichiometric combustion to begin the iterative loop, which continually updates the temperature, velocity, and mass flow profiles, until mass flow converges to a specified tolerance, $1E-8$ kg/s. A weighted average of the old and new mass flows is used to prevent overshooting in the next iteration, with a factor of 0.6 applied to the old value. Any increase in mass flow rate from the initial guess indicates inclusion of excess air due to the buoyant flow. The solution converges when the difference between mass flow rates between iterations is less than the convergence criteria, $1E-8$, requiring 10–20 iterations for most stove designs to converge. Additionally, if the pressure losses through the system are greater than the driving pressure due to buoyancy after at least 10 iterations have been completed, a no-flow error message is reported.

Heat balances

When the solution has converged, thermal efficiency is calculated per the sum of convective and radiative heat transfer into all regions

Table 3
Convective heat transfer correlations at the pot sides.

Method	Equation	Eq.	Reference
Unshielded pot			
2-D turbulent wall jet	$\mathrm{Nu} = 0.25 , \mathrm{PrRe}^{0.75}\left(\frac{z+12}{W_{jet,0}}\right)^{-0.6}$	(23)	Bussmann et al. (1983)
Forced convection laminar heated plate	$\mathrm{Nu} = 0.664\sqrt{\mathrm{Re}}$	(24)	Prasad et al. (1985)
Vertical heated plate as loss	$\tilde{h} = -1.42\left(\frac{T_p - T_{amb}}{H_p}\right)^{0.25}$	(25)	Shah and Date (2011)
Turbulent flow over isothermal plate	$\mathrm{Nu}_x = 0.0296\mathrm{Re}_x^{4/5}\mathrm{Pr}^{1/3}$	(26)	Incropera et al. (2007)
Shielded region			
Thermally developing flow in parallel plates	$\overline{\mathrm{Nu}} = 1.85\left(\mathrm{RePr}\frac{2W_{sh}}{H_{sh}}\right)^{1/3}$	(27)	Bussmann and Prasad (1986)
Constant Nusselt	$\overline{\mathrm{Nu}} = \frac{\tilde{h}\cdot W_{sh}}{k_g} = \mathrm{constant} = 4.861$	(28)	Baldwin (1987)
Optimized Format	$\overline{\mathrm{Nu}} = c_3\mathrm{Re}^{n_{13}}\left(\frac{2W_{sh}}{D_p}\right)^{n_{23}}$	(29)	
Unshielded region			
Flat plate in turbulent flow	$\mathrm{Nu}_x = 0.0296\mathrm{Re}_L^{4/5}\mathrm{Pr}^{1/3}$	(30)	Incropera et al. (2007)

Table 4
Fluid flow constants and equations

Property	Equation or value	Eq.	Reference
Friction factor in channels	Laminar $f_l = \frac{64}{Re}$	(36)	De Lepeleire et al. (1981)
	Turbulent $f_l = 0.02 - 0.09$		Moody diagram
90° turn at pot corner	$K_{bend} = 1.0$		Shah and Date (2011)
Gradual contraction	[a]$K_{cont} = 0.5$, $\sin\phi(1 - \frac{A_{i+1}}{A_i})$	(37)	Shah and Date (2011)
	[b]$K_{cont} = 0.2053 (\frac{A_i}{A_{i+1}})^2 - 0.152 \frac{A_i}{A_{i+1}}$	(38)	Shaughnessy et al. (2005)
	[c]$K_{cont} = 0.0504 (\frac{A_i}{A_{i+1}})^2 - 0.0033 \frac{A_i}{A_{i+1}}$	(39)	Shaughnessy et al. (2005)
	[d]$K_{cont} = 2.0 (\frac{A_i}{A_{i+1}})^{1/4} - 2.0$	(40)	
Gradual expansion	$K_{,exp} = (1 - \frac{A_i}{A_{i+1}})^2$	(41)	Shah and Date (2011)

[a] ϕ = half-angle of the contraction.
[b] Curve fit from tabulated values for 90° contraction at the pot side.
[c] Curve fit from tabulated values for 10° contraction at the pot bottom.
[d] Correlation that exhibited the behavior needed at the pot side.
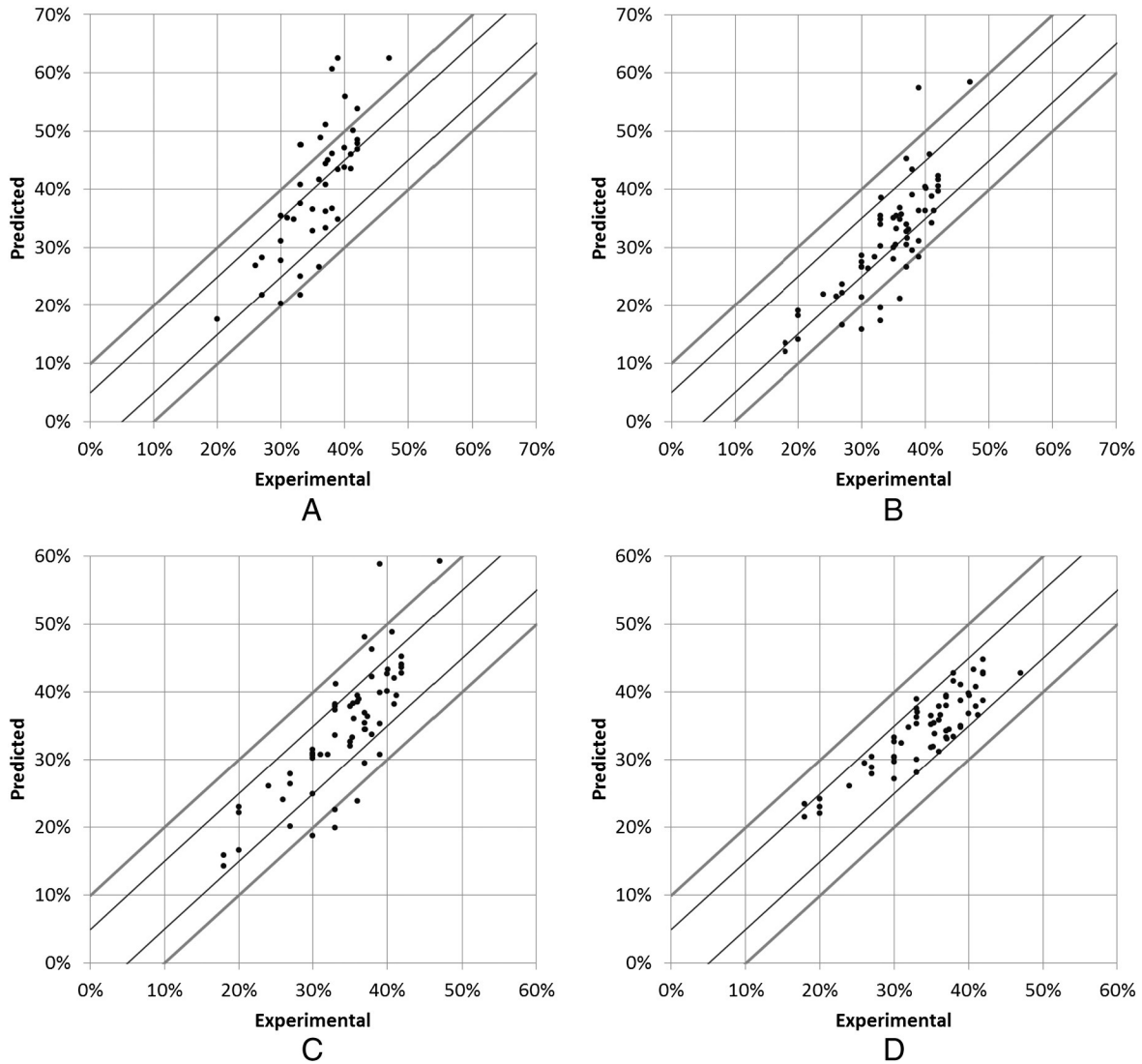
Fig. 4. Experimental vs. predicted efficiency, with bounds of ± 5%, ± 10%, per schema in Table 5: (A) Correlations from the literature, (B) Correlations from the literature with radiation tuning factor of 0.2, (C) Correlations from the literature with tuning factor of 0.2 and Nusselt correlation for the pot bottom optimized, (D) Tuning factor of 0.2 and optimized Nusselt correlations for the pot bottom and shield, and pot bottom pressure loss
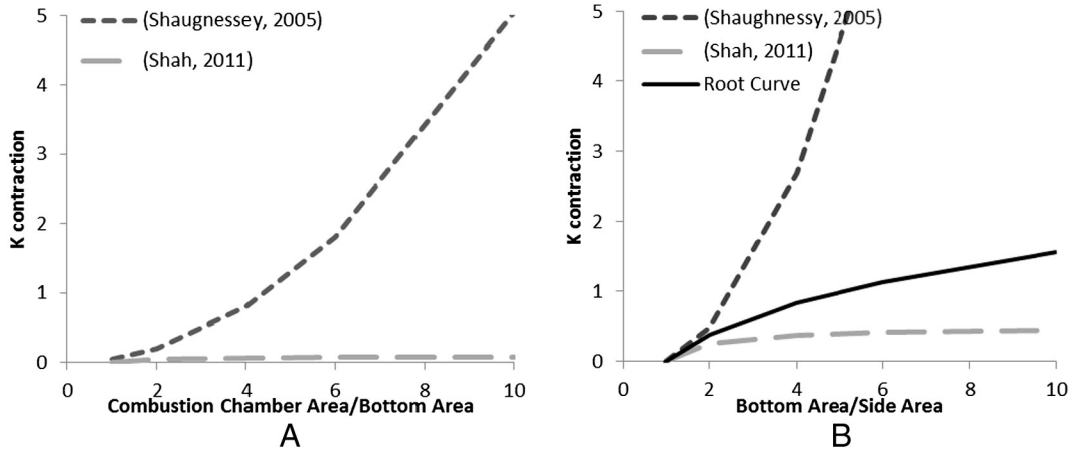
Fig. 5. K correlations (A) Pot bottom contraction, (B) Pot side contraction.

of the pot (Eq. (42)) divided by the firepower.

$$\eta = \frac{q_{pot}}{q_{wood}} \qquad (42)$$

Losses include the sum of the heat flow through the combustion chamber wall, stove top, corner, and shield. Sensible heat lost in the exiting gases is calculated in terms of the exit temperature at height of the pot water.

Model validation and verification

The model was mathematically verified by energy balance (accurate within 0.001%), investigating the effects on efficiency of changes in values for element length Δx (1 mm showing the optimal grid size), convergence criteria on the mass flow rate of gases (10^{-8} kg/s), and temperature tolerance (0.001 K) in the bisection method.

Based on a literature review of stove studies over the past 30 years, several sets of experimental laboratory results were chosen to develop the needed constants and validate the model (Bussmann and Prasad, 1986; Jetter et al., 2012; MacCarty et al., 2010). These are catalogued and analyzed by MacCarty and Bryden (2015b). The studies were chosen based on providing results for the specific type of cylindrical shielded fire stove with flat bottom pot modeled and the publishing or making otherwise available the required level of detail available on stove geometry, fuel properties, and operation. All studies used a water boiling test to measure heat transfer efficiency. This provided a consistent data set of 63 data points which include variation of all of the model design variables. Values predicted by the model were

Fig. 6. Sensitivity analysis of five geometrical design variables

compared to experimental results via the L2 norm error (Eq. (43)).

$$\varepsilon_{L2} = \sqrt{\frac{\sum_{i=1}^{N} \left(\eta_{i,pred} - \eta_{i,\exp} \right)^2}{N}} \qquad (43)$$

It should be noted that there is some uncertainty whether the model or the experimental results are the source of any discrepancies. In recent years, several international conferences, working groups, and independent studies have focused on the potential errors (Taylor, 2009), insufficient repeatability between tests (L'Orange et al., 2012) laboratories, and operators, and lack of representativeness of in-field use (Johnson et al., 2010) of the current dominant WBT protocol (Bailis et al., 2007). A 2009 analysis of the method error and uncertainty including such factors as fuel ash content, unburned char sorting, and char energy content concluded that "If results of the current UCB [University of California-Berkeley] WBT are being used to compare two stove designs, the relative error in thermal efficiency, specific fuel use, firepower, turn-down ratio, and any emissions factors expressed on a per-energy or per-mass-of-fuel-consumed basis should be assumed to be ten percent, regardless of that cited as the intra-test error" (Taylor, 2009). As such, the experimental values should be considered with an inherent potential error of at least ± 5%.

Additionally, the model is steady-state, while the experimental procedures are not. The WBT begins with the water and stove starting at ambient temperature, whereas the model assumes the pot is already at boiling temperature and the heating effects of the stove body are neglected. Thus, heat transfer to the stove body and pot will both be greater than at steady state during the water and body heating phase while mass flow will likely be reduced due to lower temperature during heating.

Table 5
Comparison of schema.

Equation and Parameter Set	Schema			
	A	B	C	D
Bottom Correlation Equation	(14)	(14)	(44)	(44)
Shield Correlation Equation	(28)	(28)	(28)	(45)
ϕ_g, ϕ_{flame}	1	0.2	0.2	0.2
K Correlation Equation	(37)	(37)	(37)	(40)
Results				
Pressure Loss > Buoyancy	19	2	2	2
Outside ± 5%	24	23	15	2
L2 Norm Error	9.0%	6.5%	5.6%	3.0%
Percent of all points within 5%	32%	60%	73%	94%

Results

Operation of the model allowed for determination of the constraint space of the model, investigation of radiation transfer and friction factor, and selection of appropriate correlations for free variables and coefficients that most accurately reflect the empirical data. The various combinations are summarized in Table 5 and Fig. 4, with discussion following.

Geometrical constraints

The method of fluid flow calculation is not appropriate for all stove geometries. Cookstoves where the diameter of the combustion chamber is greater than that of the pot, such as the Ghana Wood from (MacCarty et al., 2010), are not appropriate for the pipe model of pressure loss due to the large cross sectional area of the "pipe" in which the pot was essentially a "plug" at the pipe exit. Nor are those stoves with short combustion chambers (less than 10 cm) and no pot shield through which to develop a buoyant driving force along the flow path. Additionally, extremes in geometry such as small (5 mm) gaps around the pot can create results in which the pressure losses through the system are greater than the draft generated by buoyancy, such that the model could not run.

Radiation adjustment factor, ϕ

Many of the early models in the literature either neglected radiative heat transfer or assumed a constant fractional value of the firepower was transferred to the pot. The present model assumes blackbody radiation heat transfer with nonparticipating media, whereas in reality the view between surfaces will be partially blocked by the flame and gases including CO_2, H_2O and soot. An adjustment factor, ϕ, was added to the radiation transfers from the fuelbed, ϕ_{fl}, and gases, ϕ_g. When this factor was 1, the radiative transfer was clearly too high, shown in Fig. 4A. As shown in Table 5, the most promising pot-bottom correlations from the literature (Bussmann open fire at the pot bottom) (Eq. (11)) paired with Baldwin's constant Nu at the pot side (Eq. (27)), full radiation (ϕ = 1.0) resulted in an L2 error of 9.0%, whereas a ϕ = 0.2 shown in Fig. 4B resulted in a L2 reduction to 6.5%. More importantly, the number of configurations where the system pressure losses were greater than the buoyancy were also reduced from 19 to 2.

Laminar or turbulent friction factor

The friction factor in channels throughout the stove body was also in question due to Reynolds numbers in the transition region. For laminar flow, the Darcy friction factor is equal to 64/Re, whereas for turbulent flow it can be determined from the Moody diagram, between 0.02 and 0.09, depending on surface roughness. Testing these options in the model showed minor effects on efficiency, with the laminar correlation creating additional no-flow schemes. An optimization of the turbulent factor from 0–0.2 showed the best value to be between 0.086 and 0.1 between several runs, thus the turbulent factor equal to 0.09 was chosen as the default.

Determination and optimization of heat transfer correlations

There are five areas where multiple heat transfer coefficient correlations must be determined. The correlation for turbulent flow over an isothermal plate was deemed appropriate for both an unshielded pot and the region past an existing shield; whereas, the heat transfer correlation along the entire pot bottom and pot side within the shield were in question. Most correlations from the literature were based on experimental data and did not show suitable agreement with this more comprehensive data set, so it was a natural choice to calculate correlations in these regions based on this larger data set. A standard particle swarm optimization (PSO) was used to determine coefficients in Nusselt correlations of formats used in the literature. The PSO was run to simultaneously minimize the L2 error of predicted efficiency, the quantity of data points greater than ± 5% from the experimental data, and the number of points where the system pressure losses were greater than the draft due to buoyancy.

Several options for the format of the Nu correlation under the pot were investigated. These included the formats of Shah (Eq. (12)) and Bussmann (Eq. (11)), differentiating correlations for the pot bottom center and pot bottom above the stovetop (Eqs. (13) and (16)), and various possible characteristic lengths. A single correlation of the form of Eq. (43) provided the best results.

$$\overline{Nu}_{p,bottom} = 0.45 Re_{D_c}^{0.736} \left(\frac{D_p}{D_c}\right)^{-0.391} \tag{44}$$

After the pot bottom optimization was complete, a second PSO was run for the correlation within the shielded regions of the pot (Eq. (44)).

$$\overline{Nu}_{p,side} = 0.001 Re_{D_c}^{1.414} \left(\frac{2W_{sh}}{D_p}\right)^{0.122} \tag{45}$$

Loss coefficient for contractions

Investigation of the loss coefficients, K, for contractions in flow (Fig. 4) revealed the factor used had a significant impact on whether the pressure losses in the system would be greater than that of the buoyancy, especially for small shield gaps. For the pot bottom, the relationship from (Shah and Date, 2011) (Eq. (36)) or curve fit from (Shaughnessy et al., 2005) (Eq. (38)) both gave the same results since there were no drastic contractions under the pot bottom in the stoves tested. However, for the significant contractions at the pot side (on the order of 50% or greater), the K value was critical. It was found that the relationship in (Shah and Date, 2011) gave values that were too low thus overpredicting efficiency and the parabolic curve fit from (Shaughnessy et al., 2005) (Eq. (37)) gave too high values at these severe contractions, resulting in a no-flow situation. Upon visual investigation, it was noted that the shape of the curve needed to be a root curve, equal to 0 when the area ratio was 1, increasing more rapidly initially from 1–2, then leveling off as the area ratio continued to increase. Experimentation with values in the code showed the optimal relationship to be that of Eq. (39).

Table 6
Parameters of example simulated cookstove designs.

			Stove A	Stove B
Stove variables				
Combustion chamber diameter	D_c	(cm)	10.0	18.0
Combustion chamber height	H_c	(cm)	23.3	10.0
Gap at combustion chamber	W_c	(cm)	2.5	3.5
Gap at pot corner	W_p	(cm)	1.0	3.5
Shield gap	W_{sh}	(cm)	0.8	1.0
Stove diameter	D_{stove}	(cm)	26	18.1
Shield height	H_{sh}	(cm)	8.0	17.8
Shield thickness	t_{sh}	(cm)	0.05	0.05
Stove body conductivity	k_{stove}	(W/m·K)	1.0	26.2
Pot variables				
Pot diameter	D_p	(cm)	24.0	24.0
Pot height	H_p	(cm)	11.1	11.1
Pot volume	V_p	(L)	5.0	5.0
Fuel variables				
Fuel Heating Value	LHV_f	(MJ/kg)	19.26	18.60
Fuel Moisture Content	$MC_{f,as\text{-}rec'd}$		14%	0%
Firepower	q	(kW)	4.0	4.0

Comparison to experimental data

Results comparing the various schemes for the total 63 data points are shown in Table 5 and Fig. 4. The best correlations from the literature, including the Bussmann correlation for the pot bottom (Eq. (11)), constant Nu of 4.816 (Eq. (27)) within the pot shield (Baldwin, 1987), and full radiation is shown in Fig. 4A, with 19 points missing due to pressure losses greater than buoyancy. Fig. 4B shows that when reducing the radiation adjustment factor to 0.2 slightly underpredicts efficiency, but most importantly reduces the no-flow error points from 19 to 2 due to greater heat remaining for the buoyant flow. The optimized correlation for the pot bottom reduced the number of outliers (outside ± 5%) from 23 to 15 (Fig. 4C). Optimizing the correlation for the shielded areas of the pot and applying the improved K factor for the contraction at the side brought all but two data points to within 5%, and only two had system losses greater than buoyancy, for a total of 94% of data points predicted accurately (Fig. 4D) with an L2 norm error of 3.0%.

Simulation

Once validated as above, the model can be used to examine the effects of various design variables and to understand heat flows within the stove. Table 6 provides parameters used for simulations based on two example stove designs that were tested empirically, including (a) Stove A, the one-door rocket stove with skirt at high power tested by both Jetter et al. (2012) and MacCarty et al. (2010); and (b) Stove B, a particular variation of the metal shielded fire stove tested by (Bussmann and Prasad, 1986). An example of heat flow analysis for these stoves is provided in Table 7. Proportions agree relative to several scantly-detailed heat balances of stoves presented in (Prasad et al., 1985). The heat flow analysis shows that the two stoves have similar firepower and thermal efficiency, yet the mechanisms for heat transfer into the pot are considerably different. Only 8% of the heat transfer into the pot in Stove A is provided by radiation, while Stove B has more than twice that due to the considerably wider and shorter combustion chamber. Whereas the narrow combustion chamber and small gap under the pot in Stove A create a significant increase in convective heat transfer through the pot bottom relative to Stove B. In addition,

despite significant differences in stove body construction, with Stove A constructed of an insulative ceramic combustion chamber and Stove B of sheet metal, the stove body losses are similar. The majority of losses are represented by heat remaining in the exhaust gases, suggesting that design changes should likely focus on increasing heat transfer to the pot rather than decreasing losses from the body.

Mass flow, temperature, and resulting heat transfer coefficient and velocity data of those two stoves are shown in Table 8, which includes a comparison to rough temperature measurements taken during steady-state operation of the one-door rocket stove. Temperature comparisons show good agreement for all temperatures with the exception of the fuel bed and flame temperatures which were overpredicted and underpredicted, respectively. The mass flow through Stove B is about 33% higher than Stove A, creating increased excess air and reduced temperatures. Velocities and heat transfer coefficients in Stove B are also proportionally lower as a result.

A simulation of variable thermal conductivity for Stove A is shown in Table 9, with all variables held constant at levels in Table 6 except the stove body conductivity. The exception to this is the metal case which represents a single-walled 0.5 mm metal body with no insulation. Values for stove body conductivity are varied to represent typical cookstove combustion chamber materials. It is shown that with all other variables held constant, efficiency can be impacted by as much as 10% when moving from the most insulative (perlite) to least insulative (concrete) combustion chamber materials. Further analysis can explore the trade-offs between wall material and thickness.

The effects of varying operating conditions such as fuel moisture content, firepower, and pot diameter on Stove A are shown in Table 10, demonstrating how the model can help to predict the effects of in-field conditions on stove performance. The experimental moisture content variation of (Jetter et al., 2012) showed essentially no reduction in efficiency between dry (~10%) and wet (~20%) wood for the two rocket stoves, as did the model.

A sensitivity analysis of the five major geometrical variables for Stove A is provided in Fig. 6, indicating that the pot shield gap has the most significant impact on efficiency while the combustion chamber

Table 7
Energy balance.

	Stove A		Stove B	
	Watts	Fraction[a]	Watts	Fraction[a]
Moisture evaporation	88		0	
Equivalent daf Firepower	4024		4000	
As-received Firepower	4112		4000	
Convection				
Pot center	215	*16%*	297	*22%*
Pot bottom	699	*54%*	191	*14%*
Pot sides	391	*30%*	557	*42%*
Total Convection to Pot	1305	*92%*	1045	*79%*
Radiation				
Fire to pot	18	*15%*	212	*74%*
Wall to pot	13	*11%*	18	*6%*
Stovetop to pot	56	*49%*	16	*5%*
Shield to pot	28	*24%*	40	*14%*
Total Radiation to Pot	115	*8%*	286	*21%*
Total to Pot	1420	**35%**	1331	**33%**
Losses				
Wall	239	**6%**	124	**3%**
Stovetop	333	**8%**	122	**3%**
Corner	85	**2%**	200	**5%**
Shield	249	**6%**	302	**8%**
Sensible in Exhaust	1698	**42%**	1921	**48%**
Total Loss	2604	**65%**	2669	**67%**

[a] Italic = to pot, Bold = total.

Table 8
Flow and temperature data.

	Stove A	Measured	Stove B
Iterations	14		8
Mass flow (kg/s)	0.0049		0.0066
λ	3.7		4.9
Temperatures (°°C)			
Fuel bed	1274	790–860	1039
Flame	674	730–830	477
Pot center	470	430–590	451
Pot corner	460	320–360	428
Exit	337	230–330	303
Heat Transfer Coefficients (W/m² K)			
Pot center	45		26
Pot bottom	44		28
Average pot side	14		25
Velocities (m/s)			
Chamber	1.7		0.6
Pot side	1.5		1.5

Table 9
Insulation study.

Material	Conductivity (W/m K)	Predicted efficiency
Perlite	0.05	43.2%
Pumice	0.6	36.4%
Fireclay brick	1	35.2%
Concrete	1.7	34.3%
Metal	26.2	35.5%

Table 10
Effect of moisture content, firepower, and pot diameter.

MC$_{wood}$ (%$_{asrecd}$)	Efficiency	Firepower (W)	Efficiency	D$_p$ (m)	Efficiency
0%	36.6%	2000	31.0%		
5%	36.2%	3000	34.2%	0.16	36.0%
10%	35.9%	4000	35.9%	0.2	35.8%
15%	35.4%	5000	36.8%	0.24	35.9%
20%	35.0%	6000	37.3%		
25%	34.5%				
30%	33.9%				

diameter is the least sensitive of the five variables. These trends are also in agreement with the observations from the data set detailed in (MacCarty and Bryden, 2015b).

Conclusions and future work

The equation set presented in this paper showed good success at predicting the efficiency of a wide array of stove designs. Pairing standard equations for fluid flow in a pipe successfully indicated the flow behavior for this type of cylindrical shielded-fire stove. Several standard heat transfer correlations paired with empirical Nusselt-format optimizations derived from a large data set for the flat-bottom and shielded pot regions successfully predict 94% of measured heat transfer efficiencies within 5%. The 63 experimental data points used were the only results available with sufficient detail for validating the model, indicating a need for an accepted standard of experiments and reporting methods that are useful for modeling of such stoves. Experiments and CFD can be used to verify convective heat transfer coefficients reported by the model, as well as to verify the heat fluxes through various regions.

Although the model is able to predict heat transfer, it does not indicate the resulting combustion efficiency or practicality of the design, thus engineering judgment and experiment should be used to test the utility of any designs based on such a model. Additional research is needed to include issues of emissions including black carbon and to include models for a broader variety of cookstoves. In many cases, reduction of emissions from a cookstove is as much or more important of a goal in cookstove programs; therefore, to be fully useful the model should be updated to include solid and gas phase combustion and pollutant formation processes paired with relevant experimental data for validation.

Although many of these findings confirm what has been previously known through thumb rules, the model is able to quantify the various stove configurations without the need for extensive experiments. This will enable a broader and more thorough search of the available designs during the conceptual and preliminary design stages. Testing the model's aid in design of a new cookstove given specific constraints for community, material, and cost needs would be a good step toward investigating the power of modeling in design. Any number of design variables can be optimized in conjunction with design variables set based on user needs.

Acknowledgments

References

Agenbroad J, DeFoort M, Kirkpatrick A, Kreutzer C. A simplified model for understanding natural convection driven biomass cooking stoves—part 1: setup and baseline validation. Energy Sustain Dev 2011a;15(2):160–8.

Agenbroad J, DeFoort M, Kirkpatrick A, Kreutzer C. A simplified model for understanding natural convection driven biomass cooking stoves—part 2: with cook piece operation and the dimensionless form. Energy Sustain Dev 2011b;15(2):169–75.

Bailis R, Ogle D, MacCarty N, Still D, Smith KR, Edwards R. The Water Boiling Test, Version 3.0. Technical report. Berkeley: University of California; 2007. [pciaonline.org/node/1048 accessed 4 November 2014].

Baldwin S. Biomass stoves: engineering design, development, and dissemination [PhD Dissertation] Princeton, New Jersey: Princeton University; 1987.

Bond TC, Sun H. Can reducing black carbon emissions counteract global warming? Environ Sci Tech 2005;39:5921–6.

Bryden KM, Ashlock DA, McCorkle DS, Urban GL. Optimization of heat transfer utilizing graph based evolutionary algorithms. Int J Heat Fluid Flow 2003;24:267–77.

Burnham-Slipper H. Breeding a better stove: the use of computational fluid dynamics and genetic algorithms to optimise a wood burning stove for Eritrea [dissertation]. Nottingham, UK: University of Nottingham; 2008.

Burnham-Slipper H, Clifford MJ, Pickering SJ. Jet impingement heat transfer for low nozzle-to-plate clearances. Proc 10th UK Natl Heat Transfer Conf 2007a.

Burnham-Slipper H. A simplified wood combustionmodel for use in the simulation of cooking fires. Proc HEFAT; 2007b.

Bussmann PJT, Prasad KK. Model predictions of temperature and velocity profiles in turbulent diffusion buoyant flames. Proceedings of the 7th International Heat Transfer Conference; 1982.

Bussmann PJT, Prasad KK. Parameter analysis of a simple wood-burning cookstove. Proceedings of the 8th International Heat Transfer Conference; 1986.

Bussmann PJT, Visser P, Prasad KK. Open fires: experiments and theory. Proc Indian Acad Sci Eng Sci 1983;6(1):1–34.

Daioglou V, van Ruijven BJ, van Vuuren DP. Model projections for household energy use in developing countries. Energy 2012;38(1):601–15.

Date A. Investigation of CTARA wood-burning stove. Part II. Analytical investigation. Sadhana 1988;13(4):295–317.

De Lepeleire G, Prasad KK, Verhaart P, Visser P. A woodstove compendium. Eindhoven, the Netherlands: Eindhoven University of Technology; 1981.

Engineering Equation Solver (EES). 2011. [http://www.fchart.com/ees/ accessed 04.01.16]

Gupta R, Mittal ND. Fluid flow and heat transfer in a single-pan wood stove. Int J Eng Sci Techol 2010a;9:4312–24.

Gupta R, Mittal ND. Pyrolysis modelling in a wood stove. Int J Eng Sci Technol 2010b;2(10):5088–98.

Hannai SK, Hessari E, Fardadi M, Jeddi MK. Mathematical modeling of cooking pots' thermal efficiency using a combined experimental and neural network method. Energy 2006;31:2969–85.

Incropera FP, DeWitt DP, Bergman TL, Lavine AS. Fundamentals of heat and mass transfer. 6th ed. John Wiley & Sons; 2007.

International Energy Agency (IEA). Energy poverty: how to make modern energy access universal? Paris: World Energy Outlook; 2010.

Jetter J, Zhao Y, Smith KR, Khan B, Yelverton T, DeCarlo P, et al. Pollutant emissions and energy efficiency under controlled conditions for household biomass cookstoves and implications for metrics useful in setting international test standards. Environ Sci Technol 2012;46(19):10827–34.

Johnson NG, Bryden KM. Energy supply and use in a rural West African village. Energy 2012a;43:283–92.

Johnson NG, Bryden KM. Factors affecting woodfuel consumption in household cookstoves in an isolated rural West African village. Energy 2012b;46:310–21.

Johnson M, Edwards R, Berrueta V, Masera O. New approaches to performance testing of improved cookstoves. Environ Sci Tech 2010;44:368–74.

Kumar R, Lokras SS, Jagadish KS. Development, analysis & dissemination of a 3-pan cookstove. Bangalore: Indian Institute of Science; 1990.

Joshi J, Pandit AB, Patel SB, Singhal RS, Bhide GK, Mariwala KV, et al. Development of efficient designs of cooking systems. II Computational fluid dynamics and optimization. Ind Eng Chem Res 2012;51:1897–922.

Lim S, Vos T, Flaxman AD, Danaei G, Shibuya K, Adair-Rohani H, et al. A comparative risk assessment of burden of disease and injury attributable to 67 risk factors and risk factor clusters in 21 regions, 1990-2010: a systematic analysis for the Global Burden of Disease Study 2010. Lancet 2012;380:2224–60.

L'Orange C, DeFoort M, Willson B. Influence of testing parameters on biomass stove performance and development of an improved testing protocol. Energy Sustain Dev 2012;16:3–12.

MacCarty NA, Bryden KM. Modeling of Household Biomass Cookstoves: A Review. Energy Sustain Dev 2015a;26:1–13.

MacCarty NA, Bryden KM. A unified set of experimental data for cylindrical, natural draft, shielded single pot wood-fired cookstoves. Energy Sustain Dev 2015b;26:62–71.

MacCarty NA, Still DK, Ogle DM. Fuel use and emissions performance of fifty cooking stoves in the laboratory and related benchmarks of performance. Energy Sustain Dev 2010;14:161–71.

McCorkle DS, Bryden KM, Carmichael CG. A new methodology for evolutionary optimization of energy systems. Comput Methods Appl Mech Eng 2003;192:5021–36.

Nag PK. Heat and Mass Transfer. 2nd ed. Tata McGraw-Hill Education; 2006.

Prasad KK. Some studies on open fires, shielded fires, and heavy stoves. Eindhoven, the Netherlands: Eindhoven University of Technology; 1981.

Prasad KK, Sangen E, Visser P. Woodburning cookstoves. Advances in heat transfer, 17. Elsevier; 1985. p. 159–317.

Ragland KW, Baker AJ. Properties of wood for combustion analysis. Bioresour Technol 1991;37:161–8.

Ravi MR, Kohli S, Ray A. Use of CFD simulation as a design tool for biomass stoves. Energy Sustain Dev 2002;6(2):20–7.

Ravi MR, Sinha S, Jhalani A, Ray A. Development of a semi-empirical model for pyrolysis of an annular sawdust bed. J Anal Appl Pyrolysis 2004;71:353–74.

Rehfuess E. Fuel for life—household energy and health. Geneva, Switzerland: World Health Organization; 2006 [http://www.who.int/indoorair/publications/fuelforlife.pdf accessed 11.13.12].

Ruiz-Mercado I, Masera O, Zamora H, Smith KR. Adoption and sustained use of improved cookstoves. Energy Policy 2011;39(12):7557–66.

Shah R, Date AW. Steady-state thermochemical model of a wood-burning cook stove. Combust Sci Technol 2011;183(4):321–46.

Shaughnessy Jr EJ, Katz IM, Schaffer JP. Introduction to fluid mechanics. Oxford University Press; 2005.

Taylor III RP. The uses of laboratory testing of biomass cookstoves and the shortcomings of the dominant U.S. protocol [M.S. Thesis] Ames, Iowa, USA: Iowa State University; 2009.

Urban GL, Bryden KM, Ashlock DA. Engineering optimization of an improved plancha stove. Energy Sustain Dev 2002;6(2):9–19.

Zube DJ. Heat transfer efficiency of biomass cookstoves. Colorado State University, Fort Collins, Colorado: M.S. Thesis; 2010.

Wohlgemuth A, Mazumder S, Andreatta D. Computational heat transfer analysis of the effect of skirts on the performance of third-world cookstoves. J Therm Sci Eng Appl 2010;1. 041001-1-10.